

pubs.acs.org/macroletters Letter

Bottlebrush Elastomers with Crystallizable Side Chains: Monitoring Configuration of Polymer Backbones in the Amorphous Regions during Crystallization

Egor A. Bersenev, Evgeniia A. Nikitina, Erfan Dashtimoghadam, Sergei S. Sheiko, and Dimitri A. Ivanov*



Cite This: ACS Macro Lett. 2022, 11, 1085-1090



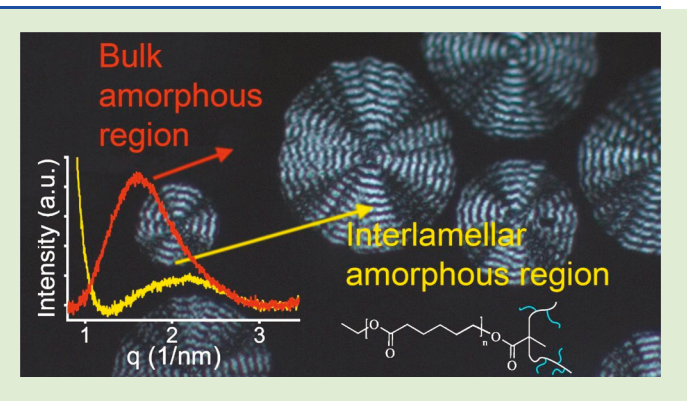
ACCESS I

III Metrics & More

Article Recommendations

s Supporting Information

ABSTRACT: Brush-like elastomers with crystallizable side chains hold promise for biomedical applications requiring the presence of two distinct mechanical states below and above body temperature: hard and supersoft. The hard semicrystalline state facilitates piercing of the body whereupon the material softens to match the mechanics of surrounding soft tissue. To understand the transition between the two states, the crystallization process was studied with synchrotron X-ray scattering for a series of brush elastomers with poly(ε -caprolactone) side chains bearing from 7 to 13 repeat units. The so-called bottlebrush correlation peak was used to monitor configuration of bottlebrush backbones in the amorphous regions during the crystallization process. In the course of crystallization, the backbones are expelled into the interlamellar amorphous gaps,



which is accompanied by their conformational changes and leads to partitioning to unconfined (melt) and confined (semicrystalline) (conformational) states. The crystallization process starts by consumption of the unconfined macromolecules by the growing crystals followed by reconfiguration of macromolecules within the already grown spherulites.

B ottlebrush polymers are unique systems where the counteraction between the backbone elasticity and steric repulsion of densely grafted side chains imposes strong effect on molecular packing and mechanical properties. Such materials hold promise for applications as photonic crystals, ^{1–3} materials for organic electronics and biomedicine. In particular, the architectural disentanglement of macromolecules allows for the design of ultrasoft and hyper-elastic materials that can replicate the deformation response of soft tissues.^{6–8} Introduction of crystallizable side chains⁹ affords thermoplastic materials with a sharp transition from a hard state to supersoft state, where the elastic modulus drops by unprecedented 6 orders of magnitude from ~1 GPa to ~1 kPa, unmatched by conventional thermoplastics. 10 Furthermore, controlling the side chain length allows tuning the melting temperature, which empowers as the design of tissue-adaptive microneedles that soften upon insertion to the body to mechanically blend with the surrounding tissue.¹⁰

Recent studies of crystallizable bottlebrushes polymers have focused on crystallization kinetics and semicrystalline morphology. The so-called bottlebrush correlation peak was observed in X-ray scattering curves at q_1^* and interpreted as an average distance between the neighboring bottlebrush backbones. In contrast to linear polymers, where interchain correlation vanishes upon melting, the bottlebrush peak

remains distinctly visible in the melt state due to side chain repulsion, which both separates the backbones and generates strong electron density contrast at the backbones. In a melt of bottlebrushes with short aliphatic side chains (up to C_{18}), the peak position, q_1^* , was shown to linearly shift with degree of polymerization (DP) of side chains, $n_{\rm sc}$. ¹⁴ However, for longer polydimethylsiloxane side chains (up to $n_{\rm sc} = 156$), the correlation becomes nonlinear and can be approximated by a scaling law with a power of 0.41.8 Upon crystallization, the appearance of the bottlebrush peak becomes strongly affected, 11 suggesting changes in the conformation and packing of bottlebrush backbones in the semicrystalline state. During side-chain crystallization, the backbones are rejected into interlamellar amorphous regions. The variation of the peak position and intensity can serve as a marker for configuration of bottlebrush backbones in amorphous regions. 15 Such information is complementary to the conventional assessment

Received: July 7, 2022 Accepted: August 16, 2022



of crystallinity and semicrystalline microstructure by wide- and small-angle X-ray scattering (WAXS and SAXS), as it adds a new dimension to the analysis of the crystallization process. This provides a unique opportunity for characterization of microstructure of confined amorphous regions that are typically inaccessible in linear chain systems. As mentioned above, linear polymers usually do not generate a distinct single-chain structure factor, which prohibits using X-ray scattering for monitoring molecular conformation in the amorphous phase of semicrystalline polymers.

So far, the state of confined interlamellar amorphous chains and its evolution during polymer crystallization process has been successfully acquired from their relaxation behavior. For example, for semirigid-chain semicrystalline polymers, it was shown that confining polymer chains in the interlamellar amorphous regions might result in significant increase of the glass transition temperature. Monitoring the relaxation behavior of such polymers during crystallization allowed observing two distinct relaxation processes, where the signal of the initial bulk amorphous phase was gradually decreasing at the expense of a new relaxation pertinent to the growing fraction of the amorphous regions confined in the intercrystal-line gaps. The modified state of the confined amorphous chains was further elucidated by transmission electron microscopy. ¹⁹

In the present work, we use the bottlebrush X-ray correlation peak to extract information about the configuration of bottlebrush backbones in a semicrystalline state (or during side-chain crystallization). This is implemented by monitoring variation of the q_1^* -peak intensity and position during crystallization process. Simultaneously, real-time characterization of the semicrystalline microstructure (thickness of the crystalline and amorphous regions, and bulk crystallinity) using the classical SAXS and WAXS data analysis.

A series of chemically cross-linked bottlebrushes with systematically varied degree of polymerization (DP) of poly(ε -caprolactone) (PCL) side chains was synthesized (Table 1). The resulting cross-link density corresponds to

Table 1. Molecular and Thermal Characteristics of the Synthesized Bottlebrush Networks

sample name	$n_{\rm sc}^{a}$	d_1^b (nm)	$T_{\rm m}^{c}$ (°C)	Τ _c (°C)	$T_{\rm m}^{d}$ (°C)	T _c ^d (°C)
PCL_7	7	3.9	20.4	-5.8	22.3	21.1
PCL_9	9	4.1	26.2	1.3	34.2	26.8
PCL_11	11	4.5	33.7	10.5	40.1	30.4
PCL_13	13	4.9	35.5	11.3	43.5	29.3

^aDP of the poly(ε -caprolactone) side chains. ^bd-spacing of the q_1^* -peak of the bottlebrush melt determined as $2\pi/q_1^*$. ^cMelting and crystallization temperatures of the bottlebrush networks. ^dThe corresponding macromonomers.

approximately one cross-link per 50 monomers of the main backbone. The details of the synthesis, the chemical structure and parameters of the molecular weight distribution are provided in the Supporting Information.

Basic thermodynamic and structural features of the synthesized bottlebrush networks were characterized by Differential Scanning Calorimetry (DSC) and SAXS (Table 1). The bottlebrush architecture imposes constraints on chain mobility during crystallization process, which explains the decrease of both melting temperature $(T_{\rm m})$ and crystallinity

compared to linear oligomers of the same length as well as the corresponding macromonomers used in the synthesis. Thus, the difference in $T_{\rm m}$ between bottlebrush elastomers and the corresponding macromonomers can reach 27 K (cf. Table 1 and Figure S2).

Figure 1 displays 1D SAXS curves of the sample with $n_{\rm sc}$ = 13 measured in the melt at 80 $^{\circ}$ C and in the semicrystalline

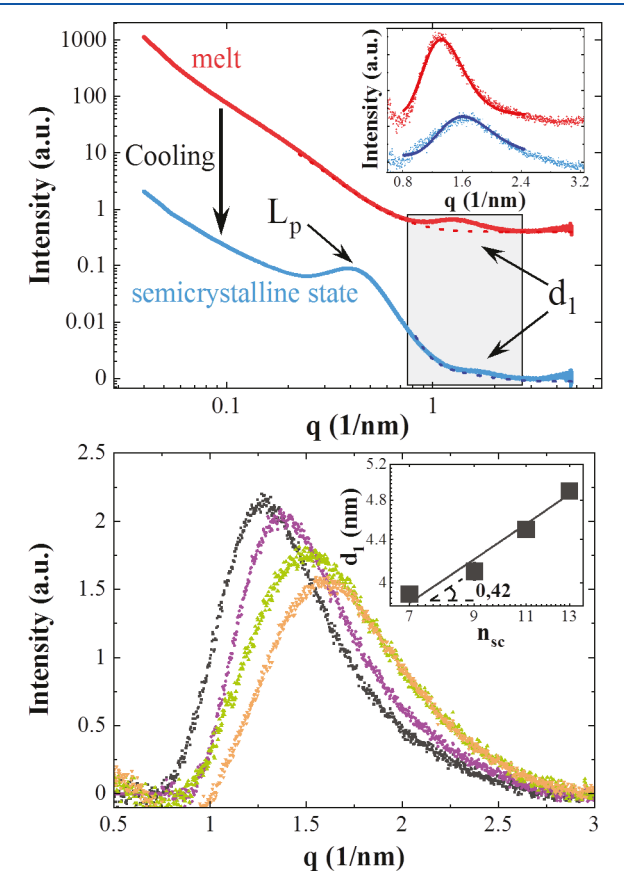


Figure 1. Top: SAXS patterns of sample PCL_13 recorded in the melt at 80 °C and after 30 min of isothermal crystallization at 20 °C. Dashed lines represent the background intensity used to correct the data. Inset shows the background-corrected regions of the curves with the bottlebrush peak shifted vertically for clarity. Bottom: 1D SAXS curves of the bottlebrush melts at 80 °C with subtracted background showing the d_1 correlation peak. The PCL_13 curve is given in black, PCL_11 in purple, PCL_9 in green, and PCL_7 in orange. Inset shows the scaling of the d_1 -spacing with the side-chain DP ($n_{\rm sc}$).

state at 20 °C. These curves exemplify two characteristic features of all studied materials: (i) bottlebrush correlation peak, d_1 , in both amorphous and semicrystalline states and (ii) Bragg peak (L_p) originated from the interference between the crystals.

By examining the bottlebrush correlation peak with more scrutiny, we can see that the peak shape and position are different for the amorphous and semicrystalline states. This difference becomes apparent in the corresponding background-corrected curves (Figure 1, inset). Upon completion of crystallization, the bottlebrush peak notably weakens, broadens, and shifts to higher q-values. Therefore, the incorporation of side chains into growing crystals causes significant modification of the bottlebrush configuration by expelling the backbones to the neighboring intercrystalline amorphous layers. The envelope of a bottlebrush polymer is likely to lose

its initial symmetrical shape due to disordering of the backbones arrangement and squeezing them closer to each other.

For the bottlebrush networks, the position of the bottlebrush peak in the melt correlates with their side-chain length (Figure 1B). The dependence of d_1 on $n_{\rm sc}$ can be approximated by a scaling law with an exponent of 0.42 ± 0.03 , which is in good agreement with the theoretical prediction mentioned in the introduction. This allows extending the observed scaling behavior to a broader family of bottlebrushes with side chains of very different chemical structure, for example, ranging from poly(dimethylsiloxane) to aliphatic polyesters.

The results of a typical isothermal melt crystallization experiment are shown in Figure 2. In the measurement, the

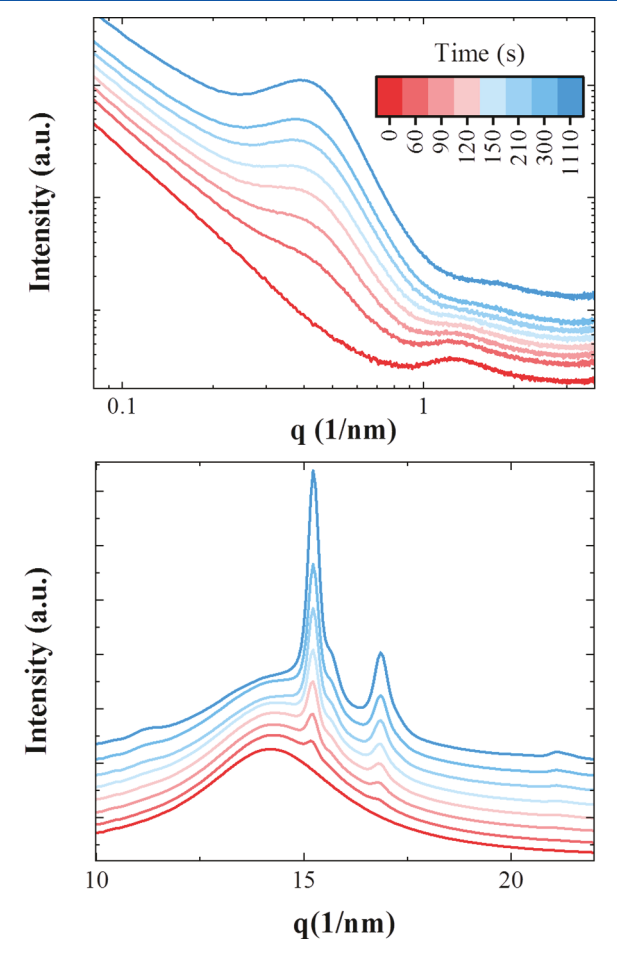


Figure 2. Selected 1D-reduced SAXS (top) and WAXS (bottom) patterns of sample PCL_13 recorded during isothermal melt crystallization at 20 $^{\circ}$ C. The color code bar represents the elapsed time of crystallization.

sample was shortly brought to the molten state at 80 °C after which it was cooled down to the temperature of crystallization at a rate of 80 °C/min. The SAXS/WAXS frames were acquired every 6 s with exposure of 6 ms. Selected timeresolved SAXS and WAXS curves show that the fast stage of crystallization completes within several minutes. The progressive increase of the $\rm L_p$ peak intensity occurs simultaneously with enhancement of the crystalline peaks' intensity in WAXS. In parallel, the changes occur in the q-region of the bottlebrush correlation peak, as discussed earlier.

To provide a quantitative description of the crystallization process based on the evolution of the bottlebrush correlation peak, the intensity in this *q*-region was approximated as a linear combination of the initial and final intensities as follows:

$$I(q, t) = \alpha(t)I_{\text{melt}}(q, t) + \beta(t)I_{\text{sc}}(q, t) + I_{\text{bckgr}}(q, t)$$
(1)

where $I_{\rm melt}$, $I_{\rm sc}$, and $I_{\rm bckgr}$ stand for the intensity of the quiescent melt before the onset of crystallization, intensity of the final semicrystalline state of the sample, and the background intensity. The functions $\alpha(t)$ and $\beta(t)$ reflect the fractions of the initial (i.e., bulk amorphous) and final (i.e., confined semicrystalline) phases contained in the sample at time t. The $I_{\rm melt}$ and $I_{\rm sc}$ were obtained by averaging about 10–20 frames and were subsequently approximated by an appropriate analytical function. The example of decomposition of the intermediate state recorded during crystallization of sample 13 at 20 °C is given in Figure 3 for the elapsed time of 220 s. At

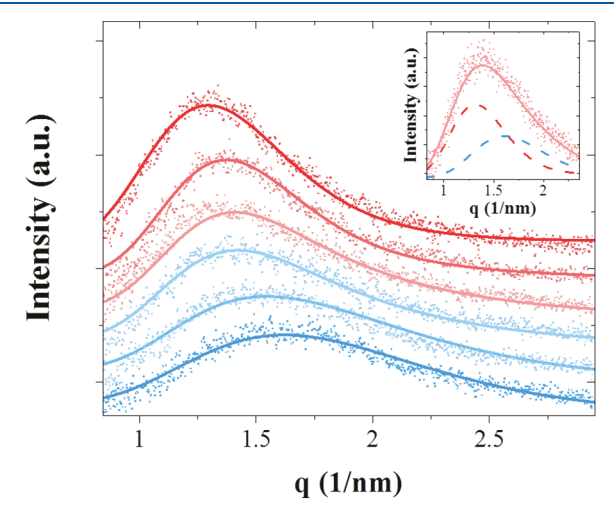


Figure 3. Variation of the bottlebrush peak during crystallization of sample PCL_13 at 20 °C. The color code is the same as in Figure 2. Experimental points are shown in dots, solid lines correspond to fits of the data with eq 1. Inset: intermediate state of the bottlebrush correlation peak at t=220 s (light gray dots). Light red solid line denotes the bottlebrush correlation peak in the melt with $\alpha=0.41$, blue solid line is intercrystalline confined state with $\beta=0.59$.

this stage of the crystallization process, the bottlebrush peak exhibits a pronounced composite character being approximately 0.4:0.6 mixture of the initial and final states.

The results of deconvolution of the SAXS intensity on the initial and final states (eq 1) are given in Figure 4A. The computed $\alpha(t)$ and $\beta(t)$ vary between 1 and 0 as expected. The progress in the crystallization process is marked by a decay of $\alpha(t)$ with simultaneous increase of $\beta(t)$. Moreover, the sum of the two functions stay close to unity at all times meaning that the intensity of the bottlebrush peak can be indeed well approximated by a linear combination of the initial and final states, that is, the I_{melt} and I_{sc} functions. As expected, the $\alpha(t)$ and $\beta(t)$ level out when all the initial amorphous phase is consumed. In the considered case this occurs after about 300 s of crystallization, which corresponds to the stage of spherulites' impingement when all the amorphous phase in the sample becomes confined. It is, therefore, clear that the bottlebrush peak provides a means to monitor the consumption of the bulk amorphous phase and its gradual replacement by the

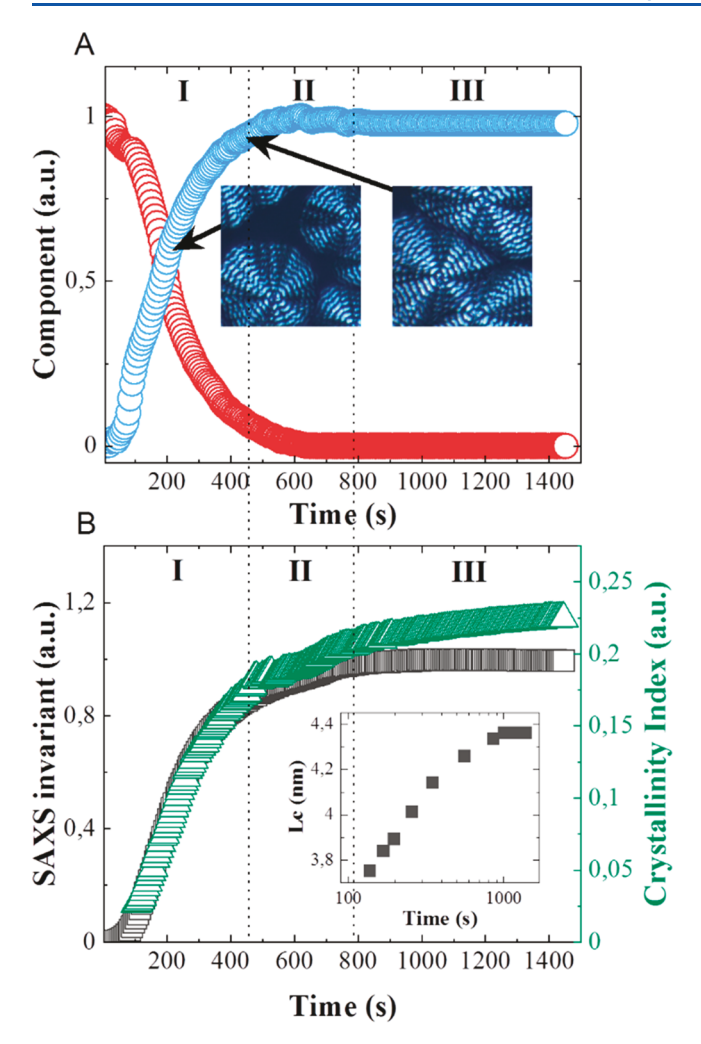


Figure 4. (A) Evolution of $\alpha(t)$ and $\beta(t)$ for isothermal crystallization of PCL ($n_{\rm sc}=13$) at 20 °C. Optical micrographs in crossed polars show growth and impingement of banded spherulites resulting from crystallization. (B) Comparative behavior of SAXS invariant (black symbols) and WAXS crystallinity index (green symbols). Inset shows the evolution of crystal thickness computed from SAXS data using 1D correlation function analysis.

amorphous regions confined in-between the crystals. This information is somehow similar to what has been achieved in the past by monitoring the intensity of the α -relaxation peak during crystallization. Here, the bottlebrush peak can also serve as a indicator allowing to discriminate and quantify the bulk and confined amorphous regions based on the configuration of the polymer chain. However, the information contained in the acquired data has broader implications discussed below.

Figure 4B displays the computed $\beta(t)$ together with the simultaneously measured SAXS invariant and WAXS crystallinity index. The three curves follow similar paths during the rapid stage of crystallization (stage I), where the bulk amorphous phase is consumed. However, upon leveling out of the $\beta(t)$ function, the SAXS invariant continues to increase for about 300 s more (stage II), suggesting that secondary crystallization processes take place within the grown spherulites. At an even later stage (stage III), when the invariant does not change anymore, the WAXS crystallinity index continues showing a slight increase. This development can be understood by analyzing the crystal thickness from the

1D correlation functions computed from SAXS data. The inset in Figure 4B shows that crystal thickness exhibits a monotonic increase, which continues even after 900 s of the isothermal crystallization process. Such slow crystal thickening in PCL was previously observed based on real-time imaging with Atomic Force Microscopy. Later, some evidence for crystal perfectioning processes was found from X-ray scattering data by Strobl and co-workers. ²¹

The described findings allow us to conclude that the crystallization process in the PCL-based bottlebrush elastomers is multistage. At the first stage, the side chains of the bottlebrush elastomers get progressively involved in the crystal growth process whereas the backbones are being rejected in the intercrystalline amorphous gaps. This is schematically illustrated in Figure 5 showing possible packing of the

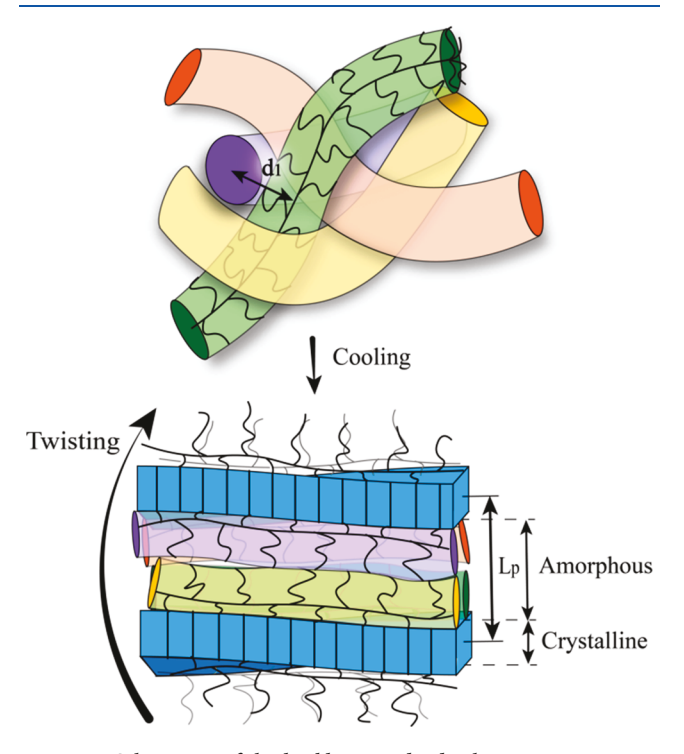


Figure 5. Schematics of the backbone and side chain arrangement in the molten and semicrystalline states.

bottlebrush backbones inside the interlamellar amorphous regions. The full consumption of the unconfined material occurs after about 450 s, which corresponds to the end of stage I. From the morphological point of view, this corresponds to impingement of growing banded spherulites of the bottlebrush as shown in the figure inserts. At stage II (up to 780 s), the entire structure formation processes occur inside the already grown spherulites. Here, the SAXS invariant still exhibits a noticeable increase (cf. Figure 4, bottom), which is likely due to some postcrystallization processes. Some of these processes continue beyond ~780 s (stage III), where the SAXS invariant levels out but the WAXS crystallinity index is still increasing (i.e., the third stage of crystallization). Importantly, the SAXS crystal thickness L_c displays a logarithmic increase throughout the whole process, which is consistent with our earlier observations on blends of linear PCL and poly(vinyl chloride).20

The computed L_c -values correspond to the crystalline stems of the length varying from about 4.5 to 5.2 repeat units, which

is slightly more than one-third of the total side-chain length. Therefore, it is logical to assume that the ends of the side chains enter lamellar crystals leaving the parts of the side chains located closer to the main backbone in the amorphous region.

To understand the universality of the described crystallization behavior, it is instructive to compare the crystallization process occurring in the studied bottlebrushes with the longest and shortest side chains, that is, for PCL samples with $n_{\rm sc} = 7$ and 13. Figure S3 shows selected SAXS and WAXS curves corresponding to isothermal melt crystallization of PCL_7 at $-10~^{\circ}$ C. Application of the same strategy for the analysis of the bottlebrush peak shows much similarity in the crystallization behavior of the two samples. Indeed, the $\alpha(t)$ and $\beta(t)$ functions add up to 1 as is the case of the PCL ($n_{sc} = 13$) crystallization (cf. Figure S5, left), which shows that the bottlebrush peak provides indeed the means of quantifying the unperturbed bulk and confined intercrystalline fraction of the bottlebrushes. Also, the crystallization process is multistage and is characterized by postcrystallization in the interior of the spherulites with a long-term thickening of the crystals. The difference in the behavior of the two samples is in the kinetics, which can be accounted for by the different degree of supercooling and in crystal thickness.

Since the remaining amorphous part of the bottlebrush molecules become smaller, the position of the bottlebrush correlation peak shifts to larger q-values. Also, perturbation of the bottlebrush packing causes the bottlebrush peak to become broader. The interlamellar amorphous regions can in principle host a couple of layers of the bottlebrush backbones as shown in the figure. The details of packing and orientation of the bottlebrush backbones are still to be explored. It is noteworthy that during melting the evolution of the bottlebrush correlation peak shows an opposite trend: the bottlebrush peak typical of the semicrystalline state vanishes and the one characteristic of the bulk polymer melt reappears as the melting process advances (cf. Figure S7).

The impact of soft confinement of the PCL side chains imposed by the bottlebrush backbones can be analyzed in comparison with hard confinement, which can be generated for example by infiltration of linear PCL into the well-studied nanoporous anodic aluminum oxide (AAO) templates.^{22,23} The walls of the AAO pores well isolate each polymer domain and can cause a dramatic depression in the PCL crystallization temperature $T_{\rm c}$. By contrast, crystallization of the bottlebrush networks studied in the present work does not show such an effect on T_c (cf. Figure S2). Therefore, contrary to the hard confinement the mechanism of crystal nucleation in the bottlebrushes is likely to be unchanged with respect to the bulk linear polymer. In our case, the resulting semicrystalline morphology of banded spherulites is typical of polymer crystallization at small and moderate undercoolings and testifies the fact that crystallization proceeds via breakout growth. In this process, the bottlebrush phase-separated morphology becomes disrupted by the growing lamellar crystals which "pass through" the interfaces delimited by the backbones and eventually trap the backbones in the interlamellar amorphous gaps.

In conclusion, the synchrotron time- and temperatureresolved SAXS and WAXS techniques with an aid of optical microscopy unveil the hierarchical organization of the bottlebrush elastomer with crystallizable side chains. Moreover, the presence of a unique bottlebrush correlation peak provides a unique probe to observe configuration of chains in the amorphous regions. Using this peak as an amorphous phase marker makes it possible to follow the consumption of the unconfined material during crystallization and address the state of the bottlebrushes in the interlamellar amorphous gaps. However, a more detailed evaluation of the structure of such crystallizable bottlebrushes is required, including nano X-ray beam diffraction experiments on the banded spherulites grown from these materials.

ASSOCIATED CONTENT

Supporting Information

The Supporting Information is available free of charge at https://pubs.acs.org/doi/10.1021/acsmacrolett.2c00394.

Materials and synthesis, NMR characterization of the bottlebrush polymers, molecular and structural parameters of the studied bottlebrush copolymers, and SAXS data treatment and analysis (PDF)

AUTHOR INFORMATION

Corresponding Author

Dimitri A. Ivanov — Faculty of Chemistry, Lomonosov Moscow State University (MSU), 119991 Moscow, Russian Federation; Institute of Problems of Chemical Physics, Russian Academy of Sciences, Moscow region 142432, Russian Federation; Institut de Sciences des Matériaux de Mulhouse-IS2M, CNRS UMR 7361, F-68057 Mulhouse, France; Sirius University of Science and Technology, 354340 Sochi, Russian Federation; orcid.org/0000-0002-5905-2652; Email: dimitri.ivanov@uha.fr

Authors

Egor A. Bersenev – Faculty of Chemistry, Lomonosov Moscow State University (MSU), 119991 Moscow, Russian Federation; Institute of Problems of Chemical Physics, Russian Academy of Sciences, Moscow region 142432, Russian Federation

Evgeniia A. Nikitina — Faculty of Chemistry, Lomonosov Moscow State University (MSU), 119991 Moscow, Russian Federation; Institute of Problems of Chemical Physics, Russian Academy of Sciences, Moscow region 142432, Russian Federation

Erfan Dashtimoghadam — Department of Chemistry, University of North Carolina at Chapel Hill, Chapel Hill, North Carolina 27599-3290, United States; Occid.org/ 0000-0001-5607-7961

Sergei S. Sheiko — Department of Chemistry, University of North Carolina at Chapel Hill, Chapel Hill, North Carolina 27599-3290, United States; orcid.org/0000-0003-3672-1611

Complete contact information is available at: https://pubs.acs.org/10.1021/acsmacrolett.2c00394

Author Contributions

*These authors contributed equally to this manuscript and have shared cofirst authorship. E.D. and S.S.S. synthesized and characterized bottlebrush elastomers; E.A.B. and E.A.N. performed synchrotron and laboratory X-ray experiments and data analysis; D.A.I. supervised the X-ray data analysis and conceived the idea of using the bottlebrush peak to monitor chain configuration in a crystallization process; D.A.I. was primary writer of the manuscript. The manuscript was written

through contributions of all authors. All authors have given approval to the final version of the manuscript. CRediT: Egor A. Bersenev data curation (equal), formal analysis (equal); Evgeniia Nikitina data curation (equal), formal analysis (equal); Erfan Dashtimoghadam data curation (equal), formal analysis (equal), investigation (equal); Sergei S Sheiko data curation (equal), formal analysis (equal), investigation (equal); Dimitri A. Ivanov conceptualization (lead), supervision (lead), writing-original draft (lead).

Notes

The authors declare no competing financial interest.

ACKNOWLEDGMENTS

E.A.B., E.A.N., and D.A.I. acknowledge financial support from the Ministry of Science and Higher Education of the Russian Federation within State Contract 075-15-2022-1117 from June 30, 2022. E.D. and S.S.S. acknowledge funding from the National Science Foundation (DMR 1921835 and DMR 2004048). The authors acknowledge perfect technical support from the personnel of the ID02 beamline of the ESRF in Grenoble (France).

REFERENCES

- (1) Sunday, D. F.; Dolejsi, M.; Chang, A. B.; Richter, L. J.; Li, R.; Kline, R. J.; Nealey, P. F.; Grubbs, R. H. Confinement and Processing Can Alter the Morphology and Periodicity of Bottlebrush Block Copolymers in Thin Films. ACS Nano 2020, 14 (12), 17476–17486.
- (2) Guo, T.; Yu, X.; Zhao, Y.; Yuan, X.; Li, J.; Ren, L. Structure Memory Photonic Crystals Prepared by Hierarchical Self-Assembly of Semicrystalline Bottlebrush Block Copolymers. *Macromolecules* **2020**, 53 (9), 3602–3610.
- (3) Zhao, T. H.; Jacucci, G.; Chen, X.; Song, D. P.; Vignolini, S.; Parker, R. M. Angular-Independent Photonic Pigments via the Controlled Micellization of Amphiphilic Bottlebrush Block Copolymers. *Adv. Mater.* **2020**, *32* (47), 2002681.
- (4) Obhi, N. K.; Jarrett-Wilkins, C. N.; Hicks, G. E. J.; Seferos, D. S. Self-Assembly of Poly(3-Hexylthiophene) Bottlebrush Polymers into End-On-End Linear Fiber Morphologies. *Macromolecules* **2020**, *53* (19), 8592–8599.
- (5) Johnson, J. A.; Lu, Y. Y.; Burts, A. O.; Xia, Y.; Durrell, A. C.; Tirrell, D. A.; Grubbs, R. H. Drug-Loaded, Bivalent-Bottle-Brush Polymers by Graft-through ROMP. *Macromolecules* **2010**, *43* (24), 10326–10335.
- (6) Dobrynin, A. V.; Rosenthal, M.; Vatankhah-Varnosfaderani, M.; Clair, C.; Magonov, S.; Sztucki, M.; Liang, H.; Cong, Y.; Ivanov, D. A.; Sheiko, S. S.; Keith, A. N. Chameleon-like Elastomers with Molecularly Encoded Strain-Adaptive Stiffening and Coloration. *Science* 2018, 359 (6383), 1509–1513.
- (7) Keith, A. N.; Vatankhah-Varnosfaderani, M.; Clair, C.; Fahimipour, F.; Dashtimoghadam, E.; Lallam, A.; Sztucki, M.; Ivanov, D. A.; Liang, H.; Dobrynin, A. V.; Sheiko, S. S. Bottlebrush Bridge between Soft Gels and Firm Tissues. *ACS Cent. Sci.* **2020**, *6* (3), 413–419.
- (8) Keith, A. N.; Clair, C.; Lallam, A.; Bersenev, E. A.; Ivanov, D. A.; Tian, Y.; Dobrynin, A. V.; Sheiko, S. S. Independently Tuning Elastomer Softness and Firmness by Incorporating Side Chain Mixtures into Bottlebrush Network Strands. *Macromolecules* **2020**, 53 (21), 9306–9312.
- (9) Yu-Su, S. Y.; Sheiko, S. S.; Lee, H.-i.; Jakubowski, W.; Nese, A.; Matyjaszewski, K.; Anokhin, D.; Ivanov, D. A. Crystallization of molecular brushes with block copolymer side chains. *Macromolecules* **2009**, *42*, 9008–9017.
- (10) Zhang, D.; Dashtimoghadam, E.; Fahimipour, F.; Hu, X.; Li, Q.; Bersenev, E. A.; Ivanov, D. A.; Vatankhah-Varnoosfaderani, M.; Sheiko, S. S. Tissue-Adaptive Materials with Independently Regulated

- Modulus and Transition Temperature. Adv. Mater. 2020, 32, e2005314.
- (11) López-Barrón, C. R.; Hagadorn, J. R.; Throckmorton, J. A. Isothermal Crystallization Kinetics of α -Olefin Molecular Bottlebrushes. *Macromolecules* **2020**, 53 (17), 7439–7449.
- (12) Sun, H.; Yu, D. M.; Shi, S.; Yuan, Q.; Fujinami, S.; Sun, X.; Wang, D.; Russell, T. P. Configurationally Constrained Crystallization of Brush Polymers with Poly(Ethylene Oxide) Side Chains. *Macromolecules* **2019**, 52 (2), 592–600.
- (13) López-Barrón, C. R.; Hagadorn, J. R.; Mattler, S. J.; Throckmorton, J. A. Syndiotactic α -Olefin Molecular Bottlebrushes: Crystallization, Melting, and Hierarchical Microstructure. *Macromolecules* **2020**, 53 (10), 3778–3788.
- (14) López-Barrón, C. R.; Tsou, A. H.; Hagadorn, J. R.; Throckmorton, J. A. Highly Entangled α -Olefin Molecular Bottlebrushes: Melt Structure, Linear Rheology, and Interchain Friction Mechanism. *Macromolecules* **2018**, *51* (17), 6958–6966.
- (15) Sarapas, J. M.; Martin, T. B.; Chremos, A.; Douglas, J. F.; Beers, K. L. Bottlebrush Polymers in the Melt and Polyelectrolytes in Solution Share Common Structural Features. *Proc. Natl. Acad. Sci. U. S. A.* **2020**, *117* (10), 5168–5175.
- (16) Ivanov, D. A.; Legras, R.; Jonas, A. M. The crystallization of poly(aryl-ether-ether-ketone) (PEEK). Interdependence between the evolution of amorphous and crystalline regions during isothermal cold-crystallization. *Macromolecules* 1999, 32, 1582–1592.
- (17) Ivanov, D. A.; Jonas, A. M.; Legras, R. The crystallization of poly(aryl-ether-ether-ketone) (PEEK). Reorganization processes during gradual reheating of cold-crystallized samples. *Polymer* **2000**, 41, 3719–3727.
- (18) Ivanov, D. A.; Jonas, A. M. Vitrification/Devitrification Phenomena during Isothermal and Nonisothermal Crystallization of Semi-Crystalline Polymers and Blends: Poly(aryl-ether-ether-ketone) (PEEK) and PEEK/ Poly(ether-imide). *Journal of Polymer Science; Part B: Polymer Physics* 1998, 36, 919–930.
- (19) Ivanov, D. A.; Pop, T.; Yoon, D.; Jonas, A. Direct space detection of order-disorder interphases at crystalline-amorphous boundaries in a semicrystalline polymer. *Macromolecules* **2002**, *35*, 9813–9818.
- (20) Basire, C.; Ivanov, D. A. Evolution of the lamellar structure during crystallization of a semicrystalline-amorphous polymer blend: time-resolved hot-stage SPM study. *Phys. Rev. Lett.* **2000**, 85, 5587–5590
- (21) Kohn, P.; Strobl, G. Continuous Changes in the Inner Order of the Crystalline Lamellae during Isothermal Crystallization of Poly(ε -Caprolactone). *Macromolecules* **2004**, 37 (18), 6823–6826.
- (22) Shi, G.; Liu, G.; Su, C.; Chen, H.; Chen, Y.; Su, Y.; Müller, A. J.; Wang, D. Reexamining the Crystallization of Poly(ε -caprolactone) and Isotactic Polypropylene under Hard Confinement: Nucleation and Orientation. *Macromolecules* **2017**, *50* (22), 9015–9023.
- (23) Safari, M.; Leon Boigues, L.; Shi, G.; Maiz, J.; Liu, G.; Wang, D.; Mijangos, C.; Muller, A. J. Effect of Nanoconfinement on the Isodimorphic Crystallization of Poly(butylene succinate-ran-caprolactone) Random Copolymers. *Macromolecules* **2020**, *53* (15), 6486–6497.